Energy Conversion

International Edition: DOI: 10.1002/anie.201913022
German Edition: DOI: 10.1002/ange.201913022

Hybrid Plasmonic–Aerogel Materials as Optical Superheaters with Engineered Resonances

*Benjamin Klemmed, Lucas V. Besteiro, Albrecht Benad, Maximilian Georgi, Zhiming Wang, Alexander Govorov, and Alexander Eychmüller**

Abstract: *Solar radiation is a versatile source of energy, convertible to different forms of power. A direct path to exploit it is the generation of heat, for applications including passive building heating, but it can also drive secondary energy-conversion steps. We present a novel concept for a hybrid material which is both strongly photo-absorbing and with superior characteristics for the insulation of heat. The combination of that two properties is rather unique, and make this material an optical superheater. To realize such a material, we are combining plasmonic nanoheaters with alumina aerogel. The aerogel has the double function of providing structural support for plasmonic nanocrystals, which serve as nanoheaters, and reducing the diffusion rate of the heat generated by them, resulting in large local temperature increases under a relatively low radiation intensity. This work includes theoretical discussion on the physical mechanisms impacting the system's balanced thermal equilibrium.*

Introduction

Under the pressure that global challenges, such as climate change, impose over our societies, the last decades have seen a surge on research efforts on the conversion of renewable sources of energy into forms that are technological useful for us. A sizeable part of this collective undertaking has been centered around the harvesting of solar energy,[1] either to generate electricity,[2] driving chemical reactions through photocatalytic processes[3–5] or harnessing it to concentrate heat.[3,6] The heat-concentration option being useful both as intermediate step in an energy-transformation process, for example, taking advantage of well-stablished engineering practices in thermoelectric generators, or having the localization or concentration of heat functioning as the desired output, for purposes such as improving dwelling habitability in cold climates or reducing its energy cost.[6]

Herein we present a high-performance hybrid material that takes advantage of the high insulating capacity of dielectric aerogels and the excellent photoheating capabilities, both in terms of efficiency and tunability, of plasmonic nanoparticles. The hybrid system combines large light-to-heat conversion efficiency, spectral tunability, very low thermal conductivity and macroscopic structural stability, making it of great interest for a range of settings, from large scale installations for solar energy-conversion[6] to tailored lab setups in a scientific context, and including other applications such as reducing the energy consumption in maintaining suitable temperatures in housing and other buildings.[6,7]

Plasmonic nanoparticles are those that support collective charge oscillations under external electromagnetic excitation, such as metallic nanocrystals, and exhibit a resonant response at particular external driving frequencies. When these resonant modes are excited, the particle couples strongly with light, manifesting large interaction cross sections. Particularly, much of the light's energy impinging on small metallic nanoparticles can be converted into heat as the plasmonic excitation dissipates non-radiatively, which has led to extensive use of plasmonic nanocrystals as efficient photothermal elements in the nanoscale,[8–12] with an emphasis in their use for targeted absorption within the biological transparency window to create localized hyperthermia for cancer treatment[13–15] and in solar-powered steam generation.[16–20] Furthermore, the well-known tuning of the plasmonic resonant frequency of a nanocrystal, be it through material composition or through its geometry, allows for systems with plasmonic structures designed to create either spectrally selective[19,21] or broad-spectrum[16,17,22] absorbers. This stands in contrast with the use of other strongly absorbing materials as photoheaters that, although having shown to be very successful as broad-spectrum photoheaters for use under solar irradiation,[23–25] they do not offer the spectral malleability of plasmonic systems. This tunability would allow to create, for instance, spectrally selective highly-sensitive bolometers,

[*] B. Klemmed, Dr. A. Benad, M. Georgi, Prof. A. Eychmüller
Physikalische Chemie
TU Dresden
Bergstrasse 66b, 01069 Dresden (Germany)
E-mail: alexander.eychmueller@chemie.tu-dresden.de
Dr. L. V. Besteiro, Prof. Z. Wang, Prof. A. Govorov
Institute of Fundamental and Frontier Sciences, University of Electronic Science and Technology of China
Chengdu 610054 (China)
Dr. L. V. Besteiro
Centre Énergie Matériaux et Télécommunications, Institut National de la Recherche Scientifique
1650 Boul. Lionel Boulet, Varennes, Quebec J3X 1S2 (Canada)
Prof. A. Govorov
Department of Physics and Astronomy, Ohio University
Athens, OH 45701 (USA)
Supporting information and the ORCID identification number(s) for the author(s) of this article can be found under: https://doi.org/10.1002/anie.201913022.

producing their output as blackbody radiation or through calorimetric measurement.

Previous work has already dealt with the assembly of plasmonic nanoparticle films[26] or the combination of plasmonic particles and other materials such as polymers,[27] wood[28] or paper[29] for application as photothermal energy converters. As reported by Gao et al., gold nanoflowers were embedded in silica hydrogels to study the low thermal conductivity of the matrix with regard to photothermal energy conversion processes.[20] However, the application of these materials in an aqueous medium leads to heat losses due to the thermal conductivity at the interfaces. In order to determine the maximum potential of plasmonic heaters, however, experiments in highly heat-insulating environments are still lacking. Therefore, herein we discuss the performance of plasmonic heaters in the heat insulating environment of an aerogel.

Aerogels are disordered porous network systems and can be obtained from a variety of materials such as metal oxides,[30] semiconductor chalcogenides[31] or mono and bimetallic noble metal nanoparticles.[32] Furthermore, investigations with mixtures of plasmonic and semiconductor nanoparticles,[33] as well as the embedding of plasmonic nanoparticles in different host materials have been reported.[34–36] However, the distribution of nanoparticles in the host material and the matching of the colloidal stability with the gelling conditions pose major challenges for the production of hybrid aerogels.[37] Metal oxide aerogels offer an ideal platform to host photothermal nanoparticles due to their low density, highly porous structure and large inner surfaces, which jointly provide a distinctly low thermal conductivity. The low thermal conductivity of metal oxide aerogels is caused by the nanoscale structure in which the finely distributed network of the metal oxide inhibits heat conduction.[38–40] In addition, and also of relevance for heating experiments, aerogels based on alumina unify high transparency, facile producibility as monolithic structures with different shapes, as well as high thermal and mechanical stability.[37–39,41,42]

Herein we report on photothermal studies of plasmonic aerogels based on gold nanorods (AuNR) into alumina aerogel. The composite material was designed to efficiently respond to a laser excitation wavelength of 650 nm. Thereby, AuNR effected the gathering and conversion of the light energy into heat and the strongly insulating aerogel hindered heat transport. Jointly, they induced the localization of thermal energy which rapidly lead to a large peak local temperature, that we monitored by a thermal camera. Furthermore, we complement the experimental results with a theoretical study to obtain a better insight into the processes taking place and the fundamental effects determining the maximum temperature of the irradiated hybrid superheater.

Through a two-stage composite synthesis with separate production of the AuNR and subsequent embedding during the gelation, the size and the shape of the AuNR were preserved. Furthermore, the optical properties of the composite gel can be adapted directly to the requirements of the thermal heating experiment. The hybrid aerogel brings the principle of the plasmonic heating AuNR to the extreme through the highly heat insulating environment of the aerogel. The heat transfer model developed on the basis of the heating experiments shows the influence of the heat insulating matrix on plasmon heating systems and is therefore potentially of interest for applications such as photothermal energy conversion processes, heating systems and sensor technology.

Results and Discussion

To obtain an effective plasmonic heater, plasmonic particles were combined with a highly insulating material (Figure 1 a,b,c). AuNR were chosen as plasmonic particles because their surface plasmon resonance can be easily adjusted to the excitation wavelength of our heating experiment by selecting the appropriate AuNR dimensions, and exemplifies the spectral tunability of the hybrid AuNR-AG material.[43] An alumina aerogel was chosen as the carrier material for the AuNR because, in addition to their large inner surface, porous structure and low density, metal oxide aerogels are also known for their low thermal conductivity.[37–39] Furthermore, alumina aerogels can be produced as transparent monolithic shaped bodies by a facile epoxy method.[41] Thus the carrier material functions as a heat insulating environment which does not interfere with the optical excitation of the AuNR for the heating experiments.

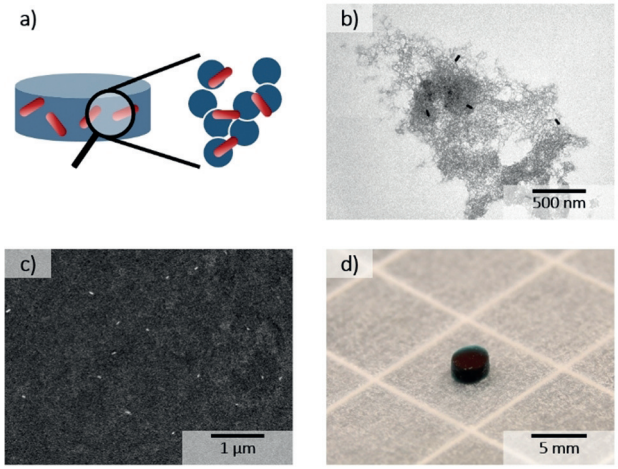

Figure 1. a) Concept sketch of the hybrid material, integration of the properties of AG (blue) and AuNRs (red). b) TEM, c) SEM in backscattered electrons mode (BSE) mode and d) photographical images of the experimental system.

The optical properties of the composite gel are dominated by the embedded AuNR, whereas the pure alumina aerogel has no special optical properties (Figure S1a in the Supporting Information). Since the absorbance of the material plays an important role in the heating experiment, it was adjusted by the concentration of embedded AuNRs. For this purpose, the composite aerogel was loaded with 1 at% Au (volume fraction 1.13×10^{-4}), resulting in an absorbance of approximately of 1.15 (see Figure S1b). Owing to their anisotropic shape, the AuNRs present two localized surface plasmon

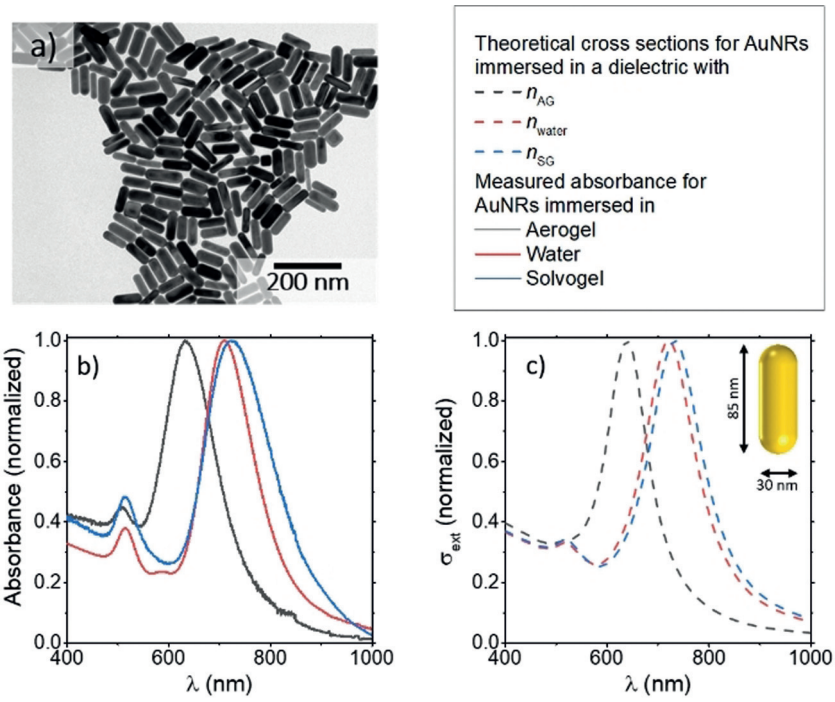

Figure 2. a) TEM image of AuNR particles from aqueous solution. b) Experimental and c) calculated absorbance spectra of AuNR in water, AuNR-Al_2O_3 solvogel in ethanol and AuNR-Al_2O_3 aerogel. The experimental ensemble contains AuNRs with an aspect ratio of 2.8. The simulation is conducted for AuNRs with a size of 85×30 nm, immersed in dielectric media with different effective permittivities: $n_{AG}=1.1$, $n_{water}=1.33$, $n_{SG}=1.36$.

resonance (LSPR) peaks in the absorption spectra. The first peak at 513 nm is attributed to the transverse mode, while the second peak at 708 nm is generated by the longitudinal one and depends on the aspect ratio of the AuNR. The experimental results showcased in Figure 2 were obtained with AuNRs with an aspect ratio of 2.8 (see Figure 2a and Figure S2a).

Besides showing the well-known sharp resonances of AuNRs, Figure 2b illustrates that the alumina superstructure, both in aerogel and in aqueous solvogel form, do not distort the optical profile of the AuNRs. As a result of the changes of the effective refractive index of the surrounding dielectric, the AuNR spectra are shifted. The simulation results shown in Figure 2c underscore this comment, as they correspond to the same AuNR in different homogeneous dielectric media. The transition from the AuNR solution to the AuNR in the solvogel leads to a red shift of the longitudinal LSPR by approximately 10 nm. By converting the solvogel into an aerogel, a blue shift of the longitudinal LSPR of approximately 90 nm occurs. In contrast, the position of the transverse LSPR remains largely unchanged by the changes in the dielectric environments. This is a well-known consequence of the elongated aspect ratios of metal NRs, in which the dipolar longitudinal mode is more susceptible to changes in the dielectric environment than the transverse one.[44–46] Furthermore, the shifts also occur to the same extent when AuNRs with different aspect ratios are embedded in the alumina gel (see Figure S3a–c).

As additional support for the possibility of increasing the loading of AuNRs into the AG, we have seen that the AuNR densities considered in this study (from 0.1 to 2.8 at%, corresponding to 1.07×10^{-5} and 3.15×10^{-4} Au volume fractions, respectively) do not appreciably broaden the absorption peaks of the sample (see Figure S3d), which indicates that the AuNRs in these samples are well dispersed and separated. Of course, this is not surprising, given that even for the sample with a 2.8 at% of gold the nanorods are still separated by 325 nm of aerogel, in average (see Figure 1c). Moreover, the low concentration of gold is clearly insufficient to significantly impact the overall thermal conductivity of the sample, thus we expect it to be fundamentally the same as the unloaded Al_2O_3 aerogel. To see this, it is helpful to consider two things: 1) the macroscopic heat transport properties in such type of hybrid materials, with particles embedded in a rigid matrix, is dominated by the component that provides connectivity to the superstructure, and even larger, regularly spaced concentrations of AuNRs would provide a hybrid material where the dominant contribution to the thermal conductivity would be the aerogel;[47] and 2) the fundamental physical factor controlling the thermal conductivity of an aerogel is the ratio between the mean free path of the gas molecules flowing through the aerogel and its average pore size, or Knudsen number,[48] and this is not affected by the inclusion of the nanoparticles, at least not until reaching very large nanoparticle volume fractions.

AuNRs have a large presence in the scientific literature due to their large optical cross sections and spectral versatility.[43] In plasmonic systems, only a fraction of the LSPR energy is dissipated through non-radiative processes that lead to localized heat generation. However, relatively small NRs, such as the ones used in this study, are efficient nanoheaters because the radiative processes represent a negligible proportion of their optical cross sections (see Figure S4). To generate heat efficiently in our experimental setup with a low density of AuNRs, we have adjusted their aspect ratio to match their LSPR frequency with that of the optical source, with a wavelength of 650 nm. However, the same concept could be used not only to achieve a different wavelength with the LSPR, but also to efficiently cover a wide spectral range by using a variety of AuNR aspect ratios or even geometries in the same sample.[49–51] The AuNR-Al_2O_3 aerogel was excited with different power densities to understand how its heating capabilities scale in circumstances akin to those of a solar concentrator. The resulting heat was monitored with a thermal imaging camera in form of temperature-time curves. A summary of the temperature-time curves and the

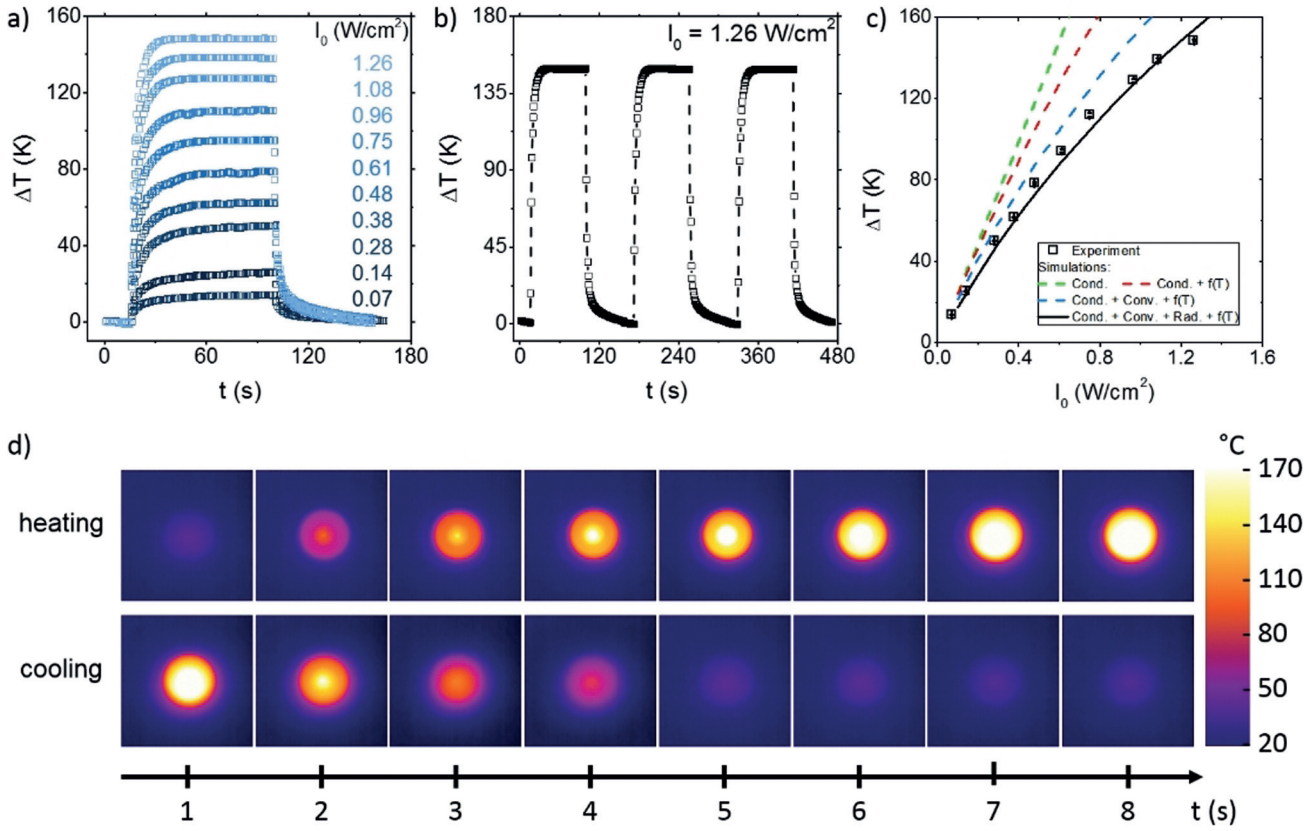

Figure 3. a) A summary of temperature-time curves at different power densities. b) Temperature–time curves at I_0 of 1.26 W cm^{-2} with identical maximum temperature. c) Measured and calculated temperature change at different excitation energies for AuNR-Al_2O_3 aerogel. The legend notes which phenomena and properties are included in the simulation: heat conduction (Cond.), convection (Conv.) and temperature-dependent material properties ($f(T)$). d) Thermographic images with top view of the AuNR-Al_2O_3 aerogel tablet. During the irradiation with the laser (power density 1.26 W cm^{-2}) the temperature rises to 170 °C. The first series of images shows the heating under illumination of the hybrid material in time intervals of 1 s. After the tablet is no longer irradiated, it cools down to room temperature. The second series of images shows the cooling of the material in time intervals of 1 s.

dependence of the temperature increase on the excitation energy is shown in Figure 3.

The progression of a temperature cycle always remains the same for any given power density because the input of energy is not large enough to cause changes in material properties. After illumination with the laser, the temperature first rises rapidly and then reaches a steady-state. In this graph we can also appreciate a qualitatively short heating and cooling times of the system, which we should understand as primarily occurring because of the very small mass of the AuNR-loaded aerogel pellet (additional discussion can be found in the Supplementary Information und Figure S5). The steady-state temperature reached under illumination is determined by the balance between the heat generation and losses. The heat generation is controlled by the laser power density and the absorbance due to the AuNRs (see Figure S1 b) that transforms a fraction of the first into heat, which is then deposited locally in the AG matrix. The heat losses acting on the pellet result from convection of the surrounding air, heat diffusion to the environment and black-body radiation. These are material- and geometry-dependent quantities that determine the temperature achieved in the steady state for a given heat generation input. Additional details on these mechanisms, and how they were implemented in the theoretical model, can be found in the Supplementary Information. To highlight the relevance of the low thermal conductivity of AG in this macroscopic system enveloping the AuNRs, we show in Figure S6 numerical results showing the dependence of the steady-state temperature on static thermal conductivity values of an hybrid pellet. Taking into account the macroscopic size of the body, it shows that the extremely low thermal conductivity of the hybrid aerogel increases the peak temperature of the system far beyond what conventional materials would produce.

After the illumination is stopped, there is a sharp drop in temperature which continues into a longer tail as the system loses its energy to the environment through the still active radiative, convective and conductive processes that represent the heat sinks in the system, until equilibrates with it and reaches room temperature. The temperature-time curves show that there is an increase in the maximum temperature in dependence of the irradiated laser power (see Figure 3 a). This progression is typical for photoheating experiments with metal nanoparticles, as in this way we scale the heat input into the system, and has already been observed with nanoparticle solutions and other composite materials.[8,9,52] Since the three

cycles recorded for one given power density always reach the same maximum temperature even at the maximum laser power density I_0 of 1.26 W cm^{-2} and since the TEM images before and after the experiment show AuNR with the same size distribution, it can be assumed that the AuNRs are mostly stable during the experiment (see Figure 3 b and Figure S7). This is of particular relevance, because it shows the viability of AuNRs as nanoheaters during sustained use at high temperatures. Furthermore, the pure alumina aerogel shows no development of heat at maximum laser power density of I_0 of 1.26 W cm^{-2}, hence it can be assumed that only the AuNR contribute to the heat generation and that there is no error in the temperature measurement due to scattering effects (see Figure S8).

From the temperature-time curves, we can study its dependence with laser power by considering the temperature increase, defined as the difference between the steady-state temperature under irradiation and room temperature. The change in temperature increases from 13.7 to 148.5 K with the increase in energy input from 0.07 to 1.26 W cm^{-2} (see Figure 3 a–c), making clear that the combination of plasmonic AuNR and the highly insulating aerogel environment results in a hybrid material capable of reaching large temperature changes with comparatively low power densities.

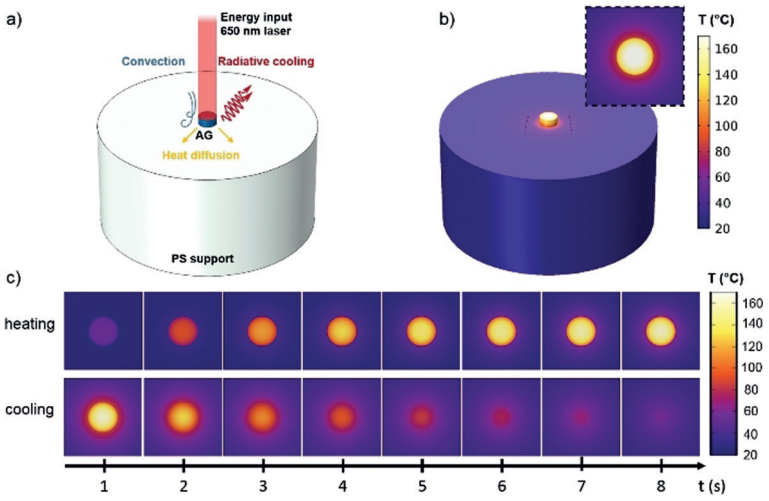

Figure 4. a) Diagram of the system used in the heat transfer calculations, with color denoting significant material differences. A cylindrical substrate of inflated polystyrene (white), with a diameter of 4 cm and a height of 2 cm, supports a cylinder of Al_2O_3 AG loaded with AuNR (cyan) with a diameter of 3.3 mm and a height of 1.4 mm. The system is heated by a laser beam that homogenously irradiates the AG disc. b) Temperature map at the different surfaces of the system, obtained through the simulation of the irradiated system's steady state. The AuNR-loaded AG has an absorbance of $A = 1.3$ and the laser intensity is $I_0 = 1.3$ W cm^{-2}. c) Details of the temperature maps, from a time-dependent simulation with the loaded AG being illuminated with a pulsed beam during 85 s. The first of the *heating* images corresponds to values of temperature 1 s after the laser pulse begins, and each subsequent image is separated in time by 1 s; the *cooling* sequence is created with the same procedure, but starting after the end of the laser pulse.

Importantly, by plotting the temperature increase versus the laser power density we observe a marked nonlinearity. As the heat input arising from the light-to-heat conversion of plasmonic nanoparticles scales linearly with I_0, we need to consider the mechanisms that bring this nonlinearity to bear in the data. As we have already shown that the AuNRs are not damaged by heating them at high laser powers (see Figure 3 b and Figure S7), this cannot be the origin of the nonlinear trend. The non-linearity of the system is based on 1) the non-linear temperature dependence of material properties, 2) radiative losses and 3) convective losses arising from air flows (see Figure 4 a). A detailed description of heat transfer simulation can be found in the Supplementary Information. Figure 3 c illustrates how the individual factors contribute to introduce a nonlinear behavior in the ΔT vs. I_0 curves, departing from the pure linearity of a system in which only heat diffusion and temperature-independent material properties are considered.

After seeing the good agreement between the experimental data and the simulation in Figure 3 c, we present an overview of the simulated system and results. Figure 4 a depicts the materials, with the AuNR-loaded AG disc modelled after the experimental sample (see Figure 1 d) and supported by a structure of inflated polystyrene, and includes schematic diagrams noting the power input -laser radiation- and outputs -heat diffusion, convection and radiative cooling- in the physical system. Whereas the theoretical data presented in Figure 3 c corresponds to the maximum temperature of the system, measured at the center of the AG disc's surface, Figure 4 b,c shows the simulated temperature maps throughout all the surfaces of the system. This representation of the theoretical results lends itself for comparison to the experimental data obtained with a thermal camera and, as such, Figure 4 c presents the computational equivalent of the observation of the heating and cooling transients captured by Figure 3 d.

Overall, Figure 3 c and a comparison between Figures 3 d and Figure 4 c indicate that we have accounted for the relevant physical mechanisms influencing the system, with the model presented thus supporting the description of the hybrid system as a light and rigid superheater. In the AuNR-AG material, the plasmonic nanorods efficiently capture light's energy and become discrete heating centers in the aerogel matrix. This Al_2O_3 scaffolding environment not only provides a structure for the AuNRs, which is also stiffer than other comparable aerogels[42] and facilitates the possibility of using this hybrid material in practical applications, but strongly limits heat diffusion due to its low thermal conductivity. This allows a large local concentration of heat, elevating the steady-state temperature of the system under irradiation. Thus, this type of hybrid superheaters can be used as versatile hot layers in experimental setups and devices, offering a high-temperature boundary under laser or solar illumination.

Conclusion

Herein we present various insights in designing and modelling efficient photoheaters using a plasmonic aerogel composite. We produced plasmonic AuNRs with resonances in an optical band that was suitable to absorb the laser used in our setup, with a wavelength of 650 nm. Subsequently, these AuNRs were embedded into highly insulating alumina aerogel pellets, allowing the hybrid system to reach a tremendous heat conversion performance. The photoheating tests were conducted under laser illumination, in which at the low intensity of 1.26 $W cm^{-2}$ a significant temperature increment of up to 148 K was observed. Under such conditions, we observed a maximum temperature of 175 °C, accompanied by a remarkable stability of the system, which retained its thermal performance after several illumination cycles and thus showed that the AuNRs withstand the high local temperatures with little to no melting. This conclusion is reinforced by the chosen experimental setup: given that we are illuminating with a monochromatic laser at a wavelength close to the longitudinal plasmonic resonance of the AuNRs—which strongly depends on the geometry of the particle—the constancy of the steady-state temperature suggests that the AuNRs size ensemble is not meaningfully modified throughout the experiment. Our discussion of the experimental results, alongside their comparison with the relevant theoretical simulations, show that the characteristic nonlinearity of the system with respect to laser intensity is well explained by a combination of radiative and convective dissipation of heat, in addition to the temperature-dependence of the properties of the materials involved. This multi-mechanistic model succeeds at explaining this nonlinearity without invoking the damaging of the AuNRs upon heating, which would be inconsistent with the thermal stability demonstrated by the system across illumination cycles. Importantly, this shows that the hybrid plasmonic-aerogel material presented here is a robust system that withstands sustained use. Jointly, these insights advance our understanding of the conversion mechanism allowing the design and modelling of novel concepts of photoheaters for a wide field of applications such as thermal power generation, solar air heating systems or including the corresponding hydrogel water purification and solar steam generation.

Acknowledgements

This project was funded by the AEROCAT ERC-grant no 340419. We thank the Department of Bioanalytical Chemistry for sharing an Optima 7000DV from PerkinElmer and R. Schulze for performing the ICP-OES measurements. We would also like to thank the Chair of Photogrammetry at TU Dresden for providing the thermal camera. L.V.B. was supported by China Postdoctoral Science Foundation (2017M622992). Z.W. was supported by National Basic Research Program of China (Project 2013CB933301) and National Natural Science Foundation of China (Project 51272038). A.O.G. was supported by the Volkswagen Foundation (Germany) and via the Chang Jiang (Yangtze River) Chair Professorship (China).

Conflict of interest

The authors declare no conflict of interest.

Keywords: energy conversion · gold nanorods · hybrid aerogel · photoheaters · surface plasmon resonance

How to cite: *Angew. Chem. Int. Ed.* **2020**, *59*, 1696–1702
Angew. Chem. **2020**, *132*, 1713–1719

[1] N. Kannan, D. Vakeesan, *Renewable Sustainable Energy Rev.* **2016**, *62*, 1092–1105.
[2] J. Khan, M. H. Arsalan, *Renewable Sustainable Energy Rev.* **2016**, *55*, 414–425.
[3] M. Romero, A. Steinfeld, *Energy Environ. Sci.* **2012**, *5*, 9234.
[4] M. Grätzel, *Nature* **2001**, *414*, 338–344.
[5] P. Lianos, *Appl. Catal. B* **2017**, *210*, 235–254.
[6] A. Saxena, Varun, A. A. El-Sebaii, *Renewable Sustainable Energy Rev.* **2015**, *43*, 863–890.
[7] R. Baetens, B. P. Jelle, A. Gustavsen, *Energy Build.* **2011**, *43*, 761–769.
[8] H. H. Richardson, M. T. Carlson, P. J. Tandler, P. Hernandez, A. O. Govorov, *Nano Lett.* **2009**, *9*, 1139–1146.
[9] H. Chen, L. Shao, T. Ming, Z. Sun, C. Zhao, B. Yang, J. Wang, *Small* **2010**, *6*, 2272–2280.
[10] M. Hu, X. Wang, G. V. Hartland, P. Mulvaney, J. P. Juste, J. E. Sader, *J. Am. Chem. Soc.* **2003**, *125*, 14925–14933.
[11] P. K. Jain, X. Huang, I. H. El-Sayed, M. A. El-Sayed, *Acc. Chem. Res.* **2008**, *41*, 1578–1586.
[12] M. B. Cortie, X. Xu, H. Chowdhury, H. Zareie, G. Smith, *Plasmonic Heating of Gold Nanoparticles and Its Exploitation*, SPIE, Bellingham, **2005**.
[13] S. Lal, S. E. Clare, N. J. Halas, *Acc. Chem. Res.* **2008**, *41*, 1842–1851.
[14] W. S. Kuo, C. N. Chang, Y. T. Chang, M. H. Yang, Y. H. Chien, S. J. Chen, C. S. Yeh, *Angew. Chem. Int. Ed.* **2010**, *49*, 2711–2715; *Angew. Chem.* **2010**, *122*, 2771–2775.
[15] T. B. Huff, L. Tong, Y. Zhao, M. N. Hansen, J. X. Cheng, A. Wei, *Nanomedicine* **2007**, *2*, 125–132.
[16] K. Bae, G. Kang, S. K. Cho, W. Park, K. Kim, W. J. Padilla, *Nat. Commun.* **2015**, *6*, 1–9.
[17] L. Zhou, Y. Tan, J. Wang, W. Xu, Y. Yuan, W. Cai, S. Zhu, J. Zhu, *Nat. Photonics* **2016**, *10*, 393–398.
[18] Y. Fu, T. Mei, G. Wang, A. Guo, G. Dai, S. Wang, J. Wang, J. Li, X. Wang, *Appl. Therm. Eng.* **2017**, *114*, 961–968.
[19] O. Neumann, A. S. Urban, J. Day, S. Lal, P. Nordlander, N. J. Halas, *ACS Nano* **2013**, *7*, 42–49.
[20] M. Gao, C. K. Peh, H. T. Phan, L. Zhu, G. W. Ho, *Adv. Energy Mater.* **2018**, *8*, 1800711.
[21] J. Yang, N. J. Kramer, K. S. Schramke, L. M. Wheeler, L. V. Besteiro, C. J. Hogan, A. O. Govorov, U. R. Kortshagen, *Nano Lett.* **2016**, *16*, 1472–1477.
[22] X. Wang, Y. He, X. Liu, G. Cheng, J. Zhu, *Appl. Energy* **2017**, *195*, 414–425.
[23] Y. Ito, Y. Tanabe, J. Han, T. Fujita, K. Tanigaki, M. Chen, *Adv. Mater.* **2015**, *27*, 4302–4307.
[24] X. Hu, W. Xu, L. Zhou, Y. Tan, Y. Wang, S. Zhu, J. Zhu, *Adv. Mater.* **2017**, https://doi.org/10.1002/adma.201604031.
[25] G. Ni, G. Li, S. V. Boriskina, H. Li, W. Yang, T. J. Zhang, G. Chen, *Nat. Energy* **2016**, *1*, 1–7.

[26] Z. Wang, Y. Liu, P. Tao, Q. Shen, N. Yi, F. Zhang, Q. Liu, C. Song, D. Zhang, W. Shang, et al., *Small* **2014**, *10*, 3234 – 3239.
[27] M. Chen, Y. Wu, W. Song, Y. Mo, X. Lin, Q. He, B. Guo, *Nanoscale* **2018**, *10*, 6186 – 6193.
[28] M. Zhu, Y. Li, F. Chen, X. Zhu, J. Dai, Y. Li, Z. Yang, X. Yan, J. Song, Y. Wang, et al., *Adv. Energy Mater.* **2018**, *8*, 1701028.
[29] Y. Liu, S. Yu, R. Feng, A. Bernard, Y. Liu, Y. Zhang, H. Duan, W. Shang, P. Tao, C. Song, et al., *Adv. Mater.* **2015**, *27*, 2768 – 2774.
[30] S. S. Kistler, *Nature* **1931**, *127*, 741.
[31] J. L. Mohanan, I. U. Arachchige, S. L. Brock, *Science* **2005**, *307*, 397.
[32] N. C. Bigall, A.-K. Herrmann, M. Vogel, M. Rose, P. Simon, W. Carrillo-Cabrera, D. Dorfs, S. Kaskel, N. Gaponik, A. Eychmüller, *Angew. Chem. Int. Ed.* **2009**, *48*, 9731 – 9734; *Angew. Chem.* **2009**, *121*, 9911 – 9915.
[33] V. Lesnyak, A. Wolf, A. Dubavik, L. Borchardt, S. V. Voitekhovich, N. Gaponik, S. Kaskel, A. Eychmüller, *J. Am. Chem. Soc.* **2011**, *133*, 13413 – 13420.
[34] J. Cai, S. Kimura, M. Wada, S. Kuga, *Biomacromolecules* **2009**, *10*, 87 – 94.
[35] P. A. Desario, J. J. Pietron, D. E. Devantier, T. H. Brintlinger, R. M. Stroud, D. R. Rolison, *Nanoscale* **2013**, *5*, 8073 – 8083.
[36] Y. Chen, K. C. Ng, W. Yan, Y. Tang, W. Cheng, *RSC Adv.* **2011**, *1*, 1265 – 1270.
[37] C. Ziegler, A. Wolf, W. Liu, A.-K. Herrmann, N. Gaponik, A. Eychmüller, *Angew. Chem. Int. Ed.* **2017**, *56*, 13200 – 13221; *Angew. Chem.* **2017**, *129*, 13380 – 13403.
[38] J. Poco, J. Satcher, L. Hrubesh, *J. Non-Cryst. Solids* **2001**, *285*, 57 – 63.
[39] J. P. Randall, M. A. B. Meador, S. C. Jana, *ACS Appl. Mater. Interfaces* **2011**, *3*, 613 – 626.
[40] G. Zu, J. Shen, X. Wei, X. Ni, Z. Zhang, J. Wang, G. Liu, *J. Non-Cryst. Solids* **2011**, *357*, 2903 – 2906.
[41] T. F. Baumann, A. E. Gash, S. C. Chinn, A. M. Sawvel, R. S. Maxwell, J. H. Satcher, *Chem. Mater.* **2005**, *17*, 395 – 401.
[42] A. Benad, F. Jürries, B. Vetter, B. Klemmed, R. Hübner, C. Leyens, A. Eychmüller, *Chem. Mater.* **2018**, *30*, 145 – 152.
[43] X. Huang, S. Neretina, M. A. El-Sayed, *Adv. Mater.* **2009**, *21*, 4880 – 4910.
[44] S. Link, M. B. Mohamed, M. A. El-Sayed, *J. Phys. Chem. B* **2002**, *103*, 3073 – 3077.
[45] C. F. Bohren, D. R. Huffman, *Absorption and Scattering of Light by Small Particles*, Wiley, Hoboken, **2008**.
[46] M. Pelton, G. W. Bryant, *Introduction to Metal-Nanoparticle Plasmonics*, Wiley, Hoboken, **2013**.
[47] W.-L. Ong, S. M. Rupich, D. V. Talapin, A. J. H. McGaughey, J. A. Malen, *Nat. Mater.* **2013**, *12*, 410 – 415.
[48] L. W. Hrubesh, R. W. Pekala, *J. Mater. Res.* **1994**, *9*, 731 – 738.
[49] H. Zhang, H. V. Demir, A. O. Govorov, *ACS Photonics* **2014**, *1*, 822 – 832.
[50] L. V. Besteiro, X.-T. Kong, Z. Wang, F. Rosei, A. O. Govorov, *Nano Lett.* **2018**, *18*, 3147 – 3156.
[51] L. V. Besteiro, K. Gungor, H. V. Demir, A. O. Govorov, *J. Phys. Chem. C* **2017**, *121*, 2987 – 2997.
[52] C. Fang, L. Shao, Y. Zhao, J. Wang, H. Wu, *Adv. Mater.* **2012**, *24*, 94 – 98.

Manuscript received: October 11, 2019
Accepted manuscript online: October 22, 2019
Version of record online: December 13, 2019

